Inconsistency in graft outcome of bilayered bioresorbable supramolecular arterial scaffolds in rats

TISSUE ENGINEERING: Part A
Volume 27, Numbers 13 and 14, 2021

DOI: 10.1089/ten.tea.2020.0185

termis
Tissue Engineering
& Regenerative Medicine
International Society

ORIGINAL ARTICLE

Inconsistency in Graft Outcome of Bilayered Bioresorbable Supramolecular Arterial Scaffolds in Rats

Renee Duijvelshoff, MD, PhD,[1,2] Andrea di Luca, PhD,[1] Eline E. van Haaften, PhD,[1] Sylvia Dekker, MSc,[1] Serge H.M. Söntjens, PhD,[3] Henk M. Janssen, PhD,[3] Anthal I.P.M. Smits, PhD,[1,2] Patricia Y.W. Dankers, PhD,[1,2] and Carlijn V.C. Bouten, PhD[1,2]

There is a continuous search for the ideal bioresorbable material to develop scaffolds for *in situ* vascular tissue engineering. As these scaffolds are exposed to the harsh hemodynamic environment during the entire transformation process from scaffold to neotissue, it is of crucial importance to maintain mechanical integrity and stability at all times. Bilayered scaffolds made of supramolecular polycarbonate-ester-bisurea were manufactured using dual electrospinning. These scaffolds contained a porous inner layer to allow for cellular infiltration and a dense outer layer to provide strength. Scaffolds ($n=21$) were implanted as an interposition graft into the abdominal aorta of male Lewis rats and explanted after 1, 3, and 5 months *in vivo* to assess mechanical functionality and neotissue formation upon scaffold resorption. Results demonstrated conflicting graft outcomes despite homogeneity in the experimental group and scaffold production. Most grafts exhibited adverse remodeling, resulting in aneurysmal dilatation and calcification. However, a few grafts did not demonstrate such features, but instead were characterized by graft extension and smooth muscle cell proliferation in the absence of endothelium, while remaining patent throughout the study. We conclude that it remains extremely difficult to anticipate graft development and performance *in vivo*. Next to rational mechanical design and good performance *in vitro*, a thorough understanding of the mechanobiological mechanisms governing scaffold-driven arterial regeneration as well as potential influences of surgical procedures is warranted to further optimize scaffold designs. Careful analysis of the differences between preclinical successes and failures, as is done in this study, may provide initial handles for scaffold optimization and standardized surgical procedures to improve graft performance *in vivo*.

Keywords: *in situ* tissue engineering, vascular graft, regeneration, bilayered polymeric scaffold, electrospinning

Impact Statement

In situ vascular tissue engineering using cell-free bioresorbable scaffolds is investigated as an off-the-shelf option to grow small caliber arteries inside the body. In this study, we developed a bilayered electrospun supramolecular scaffold with a dense outer layer to provide mechanical integrity and a porous inner layer for cell recruitment and tissue formation. Despite homogenous scaffold properties and mechanical performance *in vitro*, *in vivo* testing as rat aorta interposition grafts revealed distinct graft outcomes, ranging from aneurysms to functional arteries. Careful analysis of this variability provided valuable insights into materials-driven *in situ* artery formation relevant for scaffold design and implantation procedures.

Introduction

Cardiovascular disease has remained the leading cause of death worldwide in the last 15 years, and ~50% of these deaths emerge from coronary artery disease.[1] Surgical bypass treatment of coronary as well as peripheral artery disease requires vascular conduits, for which living, autologous vessels still represent the golden standard.[2–4] However, autologous vessels are not always available due to vascular disease, previous harvest, or when multiple or

[1]Department of Biomedical Engineering, Eindhoven University of Technology, Eindhoven, The Netherlands.
[2]Institute for Complex Molecular Systems (ICMS), Eindhoven, The Netherlands.
[3]SyMO-Chem B.V., Eindhoven, The Netherlands.

lengthy bypasses are required.[5,6] Synthetic grafts are successfully used for medium- and large-diameter vessel replacements, but often fail in the small-diameter range due to poor biocompatibility, thrombosis, and intimal hyperplasia leading to stenosis.[2,7,8] Vascular tissue engineering (TE) has the potential to fulfill the unmet clinical need for living, functional small-diameter conduits.

In the last two decades, various TE approaches have been developed to create living vascular substitutes. These techniques range from *in vitro* TE, where vessels are cultured from scaffolds and cells in the laboratory, to *in situ* TE, using cell-free scaffolds (of either biological or synthetic origin) to trigger vascular regeneration *in vivo* at the locus of implantation.[9,10] In the latter approach, a biodegradable synthetic scaffold is implanted that recruits host cells for neotissue formation, and provides mechanical support during the regeneration process until the scaffold is fully degraded and replaced.[10] Among the design parameters for biodegradable scaffolds, the choice of material and scaffold structural parameters is of pivotal importance for the success of the final construct that replaces the diseased vasculature.

An interesting group of synthetic biomaterials for vascular TE are the strictly segmented thermoplastic elastomers with supramolecularly interacting bisurea units within their structure. Their sequence-controlled macromolecular structure allows for optimal control over the nature of the polymer backbone, which subsequently affects their susceptibility to degradation and mechanical behavior.[11–13] Furthermore, these polymers are tough, allow easy surgical handling, and can be customized for specific vascular applications by incorporating noncell adhesive components, bioactive moieties, or specific cell-attracting peptides.[14–17]

In a previous study, we successfully tested tissue-engineered vascular grafts (TEVGs) made of bisurea-modified polycaprolactone scaffolds, which were strengthened by nondegradable expanded polytetrafluoroethylene.[18] However, the ultimate desire is to develop a fully biodegradable vascular TEVG as an alternative to the current nondegradable prostheses. To that end, we developed a bilayered supramolecular scaffold with a porous inner layer that allows cellular infiltration and a dense outer layer to provide strength. Based on previous *in vitro* experiments, in which we tested different bisurea-modified elastomers during accelerated degradation, we selected polycarbonate-ester-bisurea [PC(e)-BU] because of its favorable mechanical and degradative properties.[11]

This study was designed to investigate the *in vivo* performance of these bilayered supramolecular scaffolds in terms of mechanical performance and neotissue formation upon scaffold resorption. With regard to the latter, we studied whether tissue would form homogeneously and whether scaffold degradation would advance predictably *in vivo*.

Materials and Methods

Polymer synthesis and bilayered scaffold production through electrospinning

The PC(e)-BU biomaterial (Fig. 1A) (SyMO-Chem, Eindhoven, The Netherlands) was prepared as described earlier.[11]

PC(e)-BU was processed into bilayered tubular scaffolds using a dual nozzle electrospinning setup. The polymer was dissolved in either trichloromethane/hexafluoroisopropanol ($CHCl_3$:HFIP) (85/15 w/w) (Sigma-Aldrich, St. Louis, MO) (Fluorochem, Hadfield, United Kingdom) at 23% (w/w) or HFIP (Fluorochem) at 12% (w/w) to produce the inner and outer layers, respectively, and stirred overnight. After complete dissolution, the polymer solutions were dispensed with a syringe pump (PHD 22/2000; Harvard Apparatus, Holliston, MA) into a moving nozzle (0.8 mm internal diameter) placed at either 15 or 22 cm distance from the rotating collecting mandrel (1.5 mm diameter) of a climate-controlled electrospinning apparatus (EC-CLI; IME Technologies, Geldrop, The Netherlands) at 23°C and 30% relative humidity. The two distinct layers were produced according to the settings in Table 1. Total spinning time of the inner layer was 2 min, of which the last 40 s consisted of dual electrospinning of both solutions, to enable entanglement of fibers of the distinct layers. Total spinning time of the outer layer was 40 min. After removal from the mandrel, the resulting scaffolds were kept under vacuum for 16 h at 23°C to remove any residual solvents.

Scanning electron microscopy

Tubular PC(e)-BU scaffolds were examined by scanning electron microscopy (SEM; Quanta 600F; FEI, Hillsboro, OR). Samples were visualized in low vacuum atmosphere with an electron beam of 10 kV. Inner tube diameter, wall thickness, and the average fiber diameters were measured from SEM images using standard image processing software (ImageJ v1.48; U.S. NIH, Bethesda, MD). To measure fiber diameter, $\sim$30 individual fibers per layer of each sample were measured.

Explants were analyzed by SEM to visualize coverage of the scaffold with neotissue. To assess neotissue coverage and endothelialization of the implanted scaffolds, specimens were fixed in 2.5% glutaraldehyde for 24 h at 4°C and dehydrated in a graded ethanol series, starting from 50% to 100% in 5–10% increments. The ethanol was then allowed to evaporate in a vacuum chamber, and specimens were analyzed by SEM (Quanta 600F; FEI).

Biaxial tensile testing

Mechanical properties of nonimplanted control scaffolds (bilayered [$n=6$]; unilayered microporous [$n=6$]; unilayered nanoporous [$n=4$]) and explants were analyzed in wet conditions at 37°C in a biaxial tensile setup (CellScale Biomaterial Testing, Waterloo, Canada) in combination with LabJoy software (V8.01; CellScale Biomaterial Testing). Specimens were longitudinally opened, followed by thickness measurements using a digital microscope (Keyence VHX-500FE, Itasca, IL). Subsequently, the specimen's axial and circumferential directions were aligned with the actuators and mounted. Before testing, specimens were sprayed with graphite to facilitate optical strain analysis. After a precondition protocol of 10 cycles of uniaxial strain up to 10% in each direction, the samples were equibiaxially stretched at a strain rate of 100% min^{-1} until failure. Assuming incompressibility and plane-stress conditions, Cauchy stress–stretch curves were calculated from the force and displacement measurements. As a measure of stiffness, the slope of the stress–strain curve (Elastic modulus) was calculated.[19]

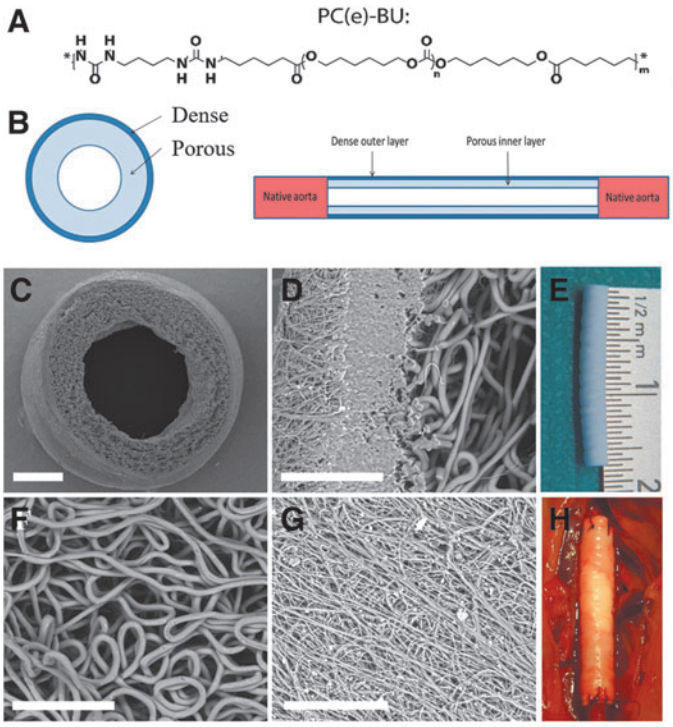

I

	Bilayered	Unilayered microporous	Unilayered nanoporous
Total wall thickness (μm)	359 ± 33	304 ± 40	323 ± 19
Inner macroporous wall thickness (μm)	270 ± 17	n.a.	n.a.
Outer nanoporous wall thickness (μm)	85 ± 26	n.a.	n.a.
Elastic modulus longitudinal (MPa)	2.63 ± 0.43	1.44 ± 0.22	2.25 ± 0.60
Elastic modulus circumferential (MPa)	1.96 ± 0.27	0.80 ± 0.08	3.06 ± 0.39

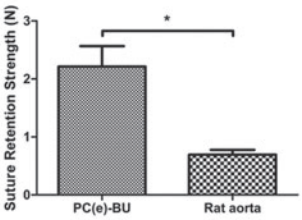

FIG. 1. Scaffold characteristics. **(A)** Chemical structure of PC(e)-BU. **(B)** Schematic representation of bilayered scaffold composition. **(C)** SEM image of bilayered scaffold preimplantation (cross-section). Scale bar represents 500 μm. **(D)** Detailed SEM image of layer intersection. Scale bar represents 50 μm. **(E)** Bilayered graft before implantation. **(F)** Detailed SEM image of microporous inner layer. Scale bar represents 50 μm. **(G)** Detailed SEM image of nanoporous outer layer. Scale bar represents 50 μm. **(H)** Bilayered graft *in situ* (infrarenal abdominal aorta of rat). **(I)** Structural characteristics and *in vitro* mechanical properties (moduli) of bilayered ($n=6$) and unilayered (macroporous [$n=6$] vs. nanoporous [$n=4$]) scaffolds. n.a.: not applicable. **(J)** Suture retention strength (N) of bilayered PC(e)-BU scaffolds ($n=5$) and rat abdominal aorta ($n=4$). *$p<0.05$. PC(e)-BU, polycarbonate-ester-bisurea; SEM, scanning electron microscopy.

Suture retention testing

Suture retention testing of bilayered scaffolds and native rat aortas was performed according to ISO 7198 ''Cardiovascular implants—Tubular vascular prostheses,'' using a tensile tester (CellScale Biomaterials Testing). In brief, samples were cut into 10-mm long segments, gripped at one extremity by a clamp, and pierced through at the other extremity by a 4–0 prolene suture (Ethicon) at a distance of 2 mm from the sample's free edge, in accordance with the standard. For the suture retention tests 4–0 prolene was chosen because previous experience taught us that 8–0 ethilon sutures (which were used for the implantations) break before the scaffold breaks. Nine samples were tested in total [$n=5$ of sterilized PC(e)-BU tubes and $n=4$ of native rat aortas]. Tests were performed in saline at 37°C. Samples were stretched at 50 mm/min until rupture. Maximum force recorded before pull-through of the suture was considered to be the suture retention strength.

Table 1. Electrospinning Settings to Produce Bilayered Scaffolds

Settings	*Inner layer*	*Outer layer*
wt% polymer	23	12
Solvent	$CHCl_3$:HFIP (85:15 w/w)	HFIP
Nozzle position[a]	Side	Top
Working distance (cm)	15	22
Voltage (kV)	18	25
Flow rate (μL/min)	80	10
Rotation speed (rpm)	200	2000
Spinning time (min)	2	40

[a]Nozzle position relative to the collecting mandrel.
$CHCl_3$:HFIP, trichloromethane/hexafluoroisopropanol.

Experimental animals

Twenty-one inbred male Lewis rats (Charles River Laboratories, Sulzfeld, Germany), weighing 298 ± 10 g, were used in this study. Animals were housed in pairs in individually ventilated cages at 20°C and 50% humidity on a 12 h light–dark cycle with *ad libitum* access to standard chow and water. After 1 week of acclimatization, 16-mm long bilayered tubular PC(e)-BU scaffolds were implanted as an interposition graft into the animals' infrarenal abdominal aorta. One animal died prematurely due to graft rupture 3 weeks postimplantation. All other animals survived until the predetermined date of sacrifice. Scaffolds were explanted after 1 month ($n=6$), 3 months ($n=7$), and 5 months ($n=7$). Part of the native abdominal aorta of each animal was explanted and used as control tissue. The animal experiments were reviewed and approved by the Animal Ethics Committee of Maastricht University (The Netherlands), and conform to the guidelines for the use of laboratory animals, as formulated by the Dutch Law on animal experimentation.

Surgical procedure

Scaffolds were sterilized by Ethylene Oxide sterilization (Synergy Health, Venlo, The Netherlands) before implantation.

Before surgery, animals were given subcutaneous analgesia (buprenorphine 0.05 mg/kg).

Operations were performed under general anesthesia (1.5–2.5% isoflurane) and under sterile conditions in spontaneously breathing animals while using an operation microscope (Leica Microsystems, Wetzlar, Germany). Body temperature was maintained at 37°C using a heating pad. Animals were administered 25 IE of heparin subcutaneously before surgery. After a midline laparotomy, the aorta was separated from the inferior vena cava and surrounding tissues. The segment of the abdominal aorta between the renal arteries and the aortic bifurcation was mobilized, collateral branches tied using 6–0 silk (Braun Aesculap, Tuttlingen, Germany), followed by aortic crossclamping of the aorta between the renal arteries and the bifurcation with microvascular clamps. The aorta was transected, and scaffolds were placed as an interposition graft with end-to-end anastomosis performed at both the proximal and the distal ends using interrupted 8–0 nylon sutures (Ethilon®; Ethicon, Johnson & Johnson, New Brunswick, NJ). When the clamps were removed and hemostasis was achieved, the aorta was closely inspected to confirm pulsatile flow distal to the tubular scaffold. The abdomen was closed in two layers using 4–0 sutures (Vicryl®; Ethicon, Johnson & Johnson). Animals recovered in a recovery chamber at 30°C and were assessed for evidence of acute failure, before returning to their cage. At the end of the day of surgery, animals were given subcutaneous analgesia (buprenorphine 0.05 mg/kg), which was continued twice daily during the first three postoperative days. No anticoagulation or antiplatelet therapy was given throughout the duration of the study. In addition to standard chow, animals received recovery dietgels (ClearH2O®, Westbrook, ME) for 3 days postoperatively, to improve their recovery.

On the predetermined day of sacrifice, animals were euthanized under isoflurane anesthesia by exsanguination. First, the aorta was closely inspected to confirm pulsatile flow distal to the tubular scaffold. Animals were then systematically perfused with cold phosphate-buffered saline (PBS) (Sigma-Aldrich), after which the scaffold and a native aorta control specimen were carefully explanted.

Histology

Specimens were fixed in 3.7% formalin for 24 h at 4°C, and embedded in optimal cutting temperature compound (Tissue-Tek®; Sakura Finetek Europe B.V., Alphen aan den Rijn, The Netherlands). Five micrometers thick sections were cut and mounted on Polysine® glass slides (ThermoFischer Scientific, Waltham, MA). Slides were washed in PBS and stained with Russell-Movat pentachrome (American MasterTech, Lodi, CA) to assess gross morphology and tissue composition. Alizarin Red S (Sigma-Aldrich) stains were performed to assess calcium deposits. Stained slides were then dehydrated by quick exposure to a graded series of ethanol solutions (70–100%) and mounted in Entellan (Merck, Darmstadt, Germany). No xylene was used during the protocol to prevent damage to the polymeric fibers. Tile scans and pictures were recorded with a Zeiss Axio 681 Observer Z1 microscope (Carl Zeiss Microscopy GmbH, Jena, Germany).

Immunohistochemistry

Specimens were fixed, embedded, and cut as described in the previous section. Slides were washed in PBS, and antigen retrieval was performed in a 96°C water bath for 20 min in citrate buffer (pH 6.1: DAKO) followed by a permeabilization step with 0.5% Triton-X-100 (Merck) in PBS for 10 min at room temperature. Blocking was performed by incubating slides in 1% nonfat dry milk, 1% BSA, 2% normal goat serum (Invitrogen, Carlsbad, CA), and 0.3 M Glycin (Sigma-Aldrich) in 0.05% Tween-20 (Merck) in PBS for 1.5 h at room temperature in a humidified chamber.

Primary antibodies were prepared at the desired concentrations in 1:10 diluted blocking buffer and were applied overnight at 4°C in a humidified chamber. The primary antibodies used were as follows: mouse anti-α-smooth muscle actin (α-SMA) (1:600; Sigma-Aldrich) and rabbit anti-von Willebrand Factor (vWF) (1:1000; Abcam, Cambridge, United Kingdom). All washing steps were done with 0.05% Tween-20 in PBS. The following day, slides were washed and incubated with Alexa Fluor 488/647 secondary antibodies (1:500; Molecular Probes, ThermoFischer Scientific) for 1.5 h at room temperature in a humidified chamber. Cell nuclei were stained with 4′,6-diamidino-2-phenylindole (DAPI). Omitting the primary antibody from the staining procedure generated negative control sections. Stained slides were mounted in Mowiol (Calbiochem, San Diego, CA) and visualized with a Zeiss Axiovert fluorescence microscope (Carl Zeiss Microscopy GmbH).

Gel permeation chromatography

To analyze remaining scaffold in explants by gel permeation chromatography (GPC), neotissue was removed by incubating the explants with 5% sodium hypochlorite solution (clorox) for 15 min at room temperature. After incubation, samples were washed three times in purified water, and dried overnight in a vacuum oven at 37°C. Subsequently, scaffold samples were dissolved in dimethylformamide, supplemented with 10 mM LiBr and 0.25% (v/v) H_2O, at a concentration of 1 mg/mL. Before measurement, the samples were filtered over a 0.2-μm regenerated cellulose filter. Weight averaged molecular weights (M_w) and number averaged molecular weights (M_n) were determined with a Varian/Polymer Laboratories PL-GPC 50 Plus instrument (Varian, Inc., Palo Alto, CA) operated at 50°C equipped with a Shodex GPC KD-804 column (Shodex, Tokyo, Japan), relative to polyethylene glycol standards.

Statistical analysis

Data are expressed as mean ± standard deviation, with the exception of the mechanical data of the explants, which is expressed as mean ± standard error of the mean. All datasets were tested for normality using the Shapiro–Wilk test, which confirmed a non-normal distribution of the data due to the limited sample size. Therefore, we used nonparametric tests for statistical analysis. Biaxial tensile data were analyzed with the Kruskal–Wallis test, followed by Dunn's

multiple comparison test. Suture retention data were analyzed with the Mann–Whitney test. Statistical analyses were performed with Prism software (Graphpad Software v5.04, La Jolla, CA); differences were considered to be statistically significant for p-values <0.05.

Results

Bilayered scaffolds show anisotropic mechanical behavior with the outer nanoporous layer providing stiffness to the scaffold

Dual electrospinning resulted in bilayered scaffolds, with an inner diameter of 1.54 ± 0.03 mm and a total wall thickness of 461 ± 32 μm (Fig. 1B–E). The scaffolds consistently showed a porous microstructure of the inner layer (fiber diameter of 2.77 ± 0.29 μm) and dense nanostructure of the outer layer (fiber diameter of 0.60 ± 0.05 μm) (Fig. 1F, G). *In vitro* biaxial tensile tests showed that bilayered grafts ($n = 6$) were stiffer in the longitudinal direction (2.63 ± 0.43 MPa) than in the circumferential direction (1.96 ± 0.27 MPa) (Fig. 1I). Suture retention strength of bilayered scaffolds was significantly higher than native rat aorta (2.21 ± 0.32 N vs. 0.70 ± 0.07 N), and comparable with human saphenous vein and human artery as described elsewhere (Fig. 1J).[20,21]

Most explants exhibit aneurysmal changes with a large interindividual variation in overall appearance

Macroscopically, explants showed great interindividual variability despite homogeneity in the experimental group and scaffold production (Fig. 2A). Most of the grafts exhibited aneurysm formation. The explant's maximal external diameters were 3.5 ± 0.9, 4.8 ± 2.4, or 4.6 ± 1.6 mm after 1, 3, and 5 months, respectively (for individual values see Fig. 2B). Lengths of explants were 16.7 ± 1.1, 18.6 ± 2.4, or 17.6 ± 2.9 mm after 1, 3, and 5 months, respectively (for individual values see Fig. 2C). Strikingly, two of the three explants that did not show aneurysm formation had increased in length by 1.5-fold when compared with the initial scaffold length (16 mm) (Fig. 2).

Nonaneurysmatic explants are characterized by wall thickening and muscular composition

The midsection wall thickness of explants remained relatively constant in time, with thicknesses of 513.06 ± 46.75, 535.04 ± 101.79, and 511.74 ± 70.94 μm after 1, 3, and 5 months, respectively. The two explants from the 3 months group that did not demonstrate enlargement in maximal external diameter were analyzed separately, and displayed a considerably higher wall thickness of 613.90 ± 87.40 μm (Fig. 3).

Russell-Movat pentachrome staining revealed that 3 months nonaneurysmatic explants displayed a muscular composition, whereas their 3 months aneurysmatic counterparts displayed a composition rich in glycosaminoglycans. Five months explants were mainly composed of collagen, although glycosaminoglycans and muscle tissue were also present (Fig. 3).

SEM demonstrated neotissue formation with a native-like organization in both 3 and 5 months explants with no sign of scaffold present (Fig. 4). One month explants mainly displayed scaffold (data not shown).

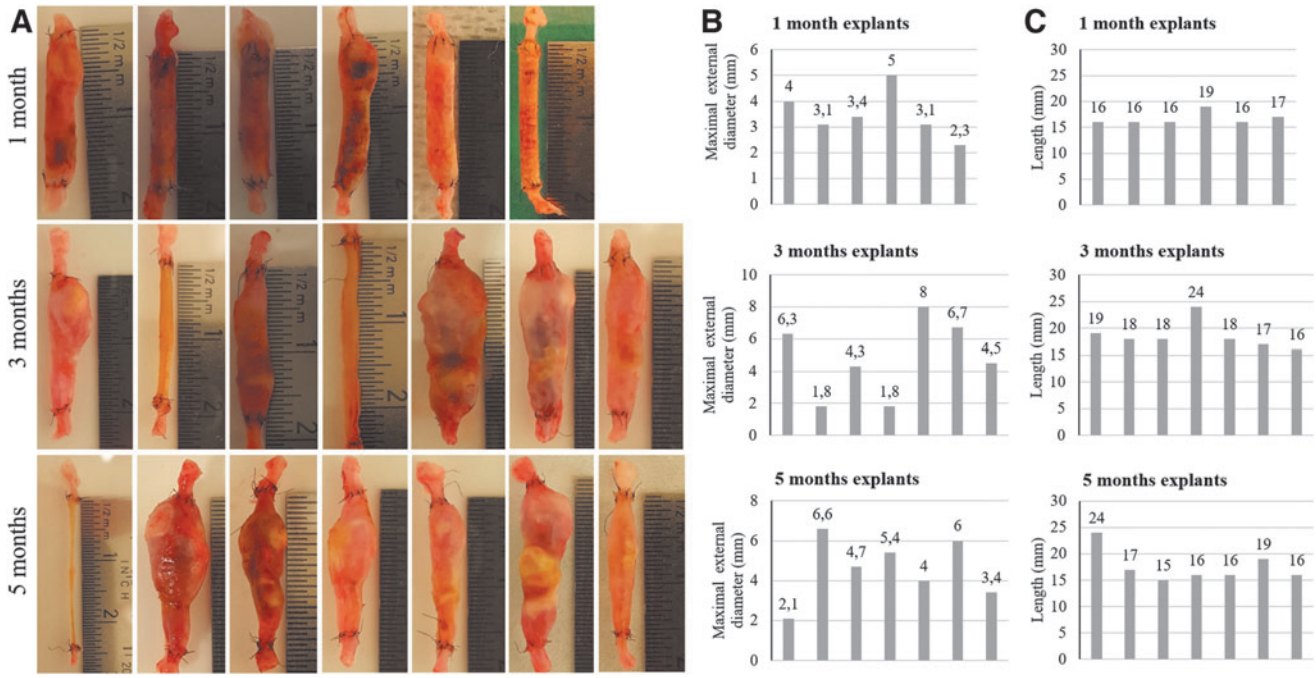

FIG. 2. Macroscopic features of explants. **(A)** Interindividual variability of explants. **(B)** Maximal external diameter of individual explants in mm. **(C)** Length of individual explants in mm. Note: order of pictures in each *row* in **(A)** are consistent with the order of bars in the same *row* in **(B, C)**.

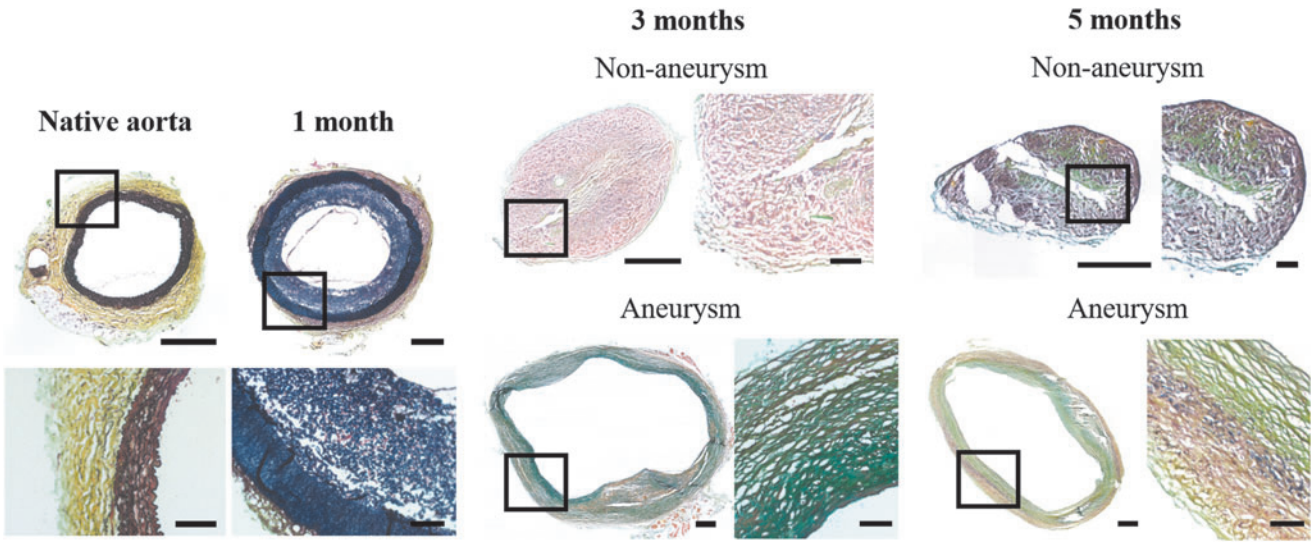

FIG. 3. Matrix/tissue development. Russell-Movat pentachrome staining (*black*: elastic fibers, nuclei; *red*: muscle; *yellow*: collagen; intense *red*: fibrinoid; *blue* to *green*: mucins). Scale bars represent 500 μm for the cross-sections of aorta and explants (images with a box). Scale bars represent 100 μm for the zoom images of aorta and explants (images without a box).

Aneurysmatic 3 and 5 months explants stain positive for calcium

Alizarin Red S staining was used to detect the presence of calcium in explants. None of the 1 month explants displayed presence of calcium. Of the 3 months explants, all explants that exhibited aneurysmal deformation (five of seven) displayed presence of calcium, and of the 5 months explants all except for one (six of seven) (Fig. 5). In the explants that did not show aneurysm formation, no calcium was detected.

Explants display tissue-like nonlinear elastic behavior

Starting from an almost linear elastic material behavior of the PC(e)-BU bilayered scaffolds, the explants displayed

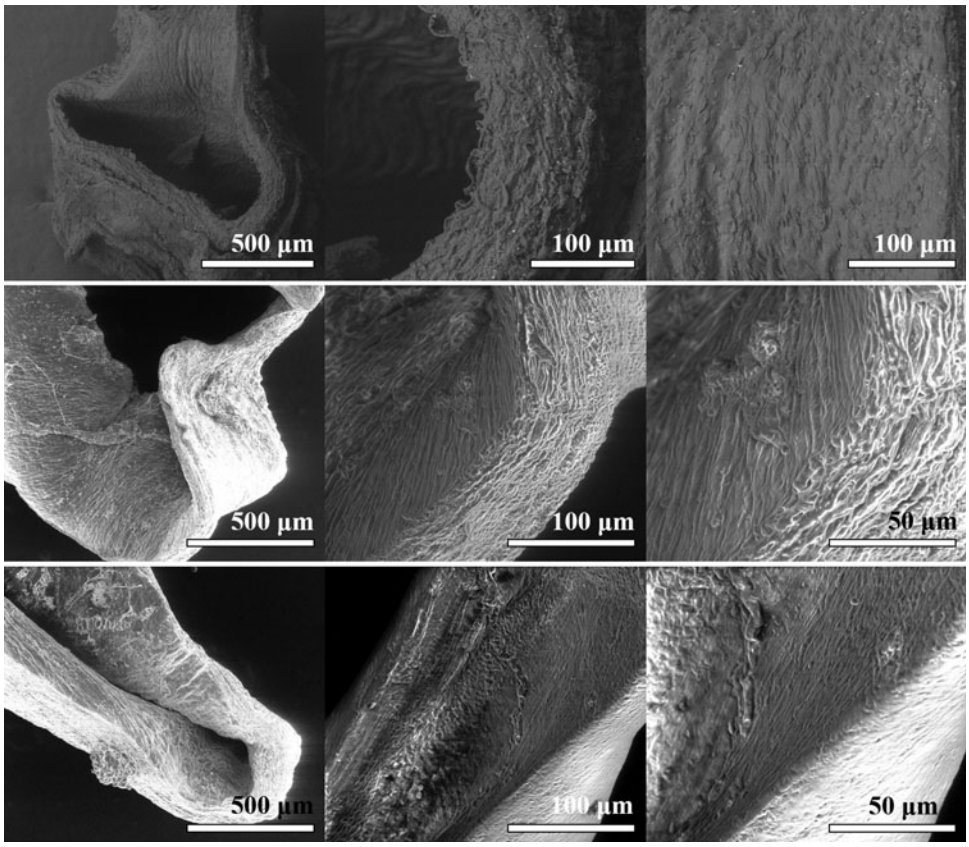

FIG. 4. Neotissue formation at microscopic level. SEM images. *Upper row*: native rat aorta. *Middle row*: 3 months explant. *Lower row*: 5 months explant.

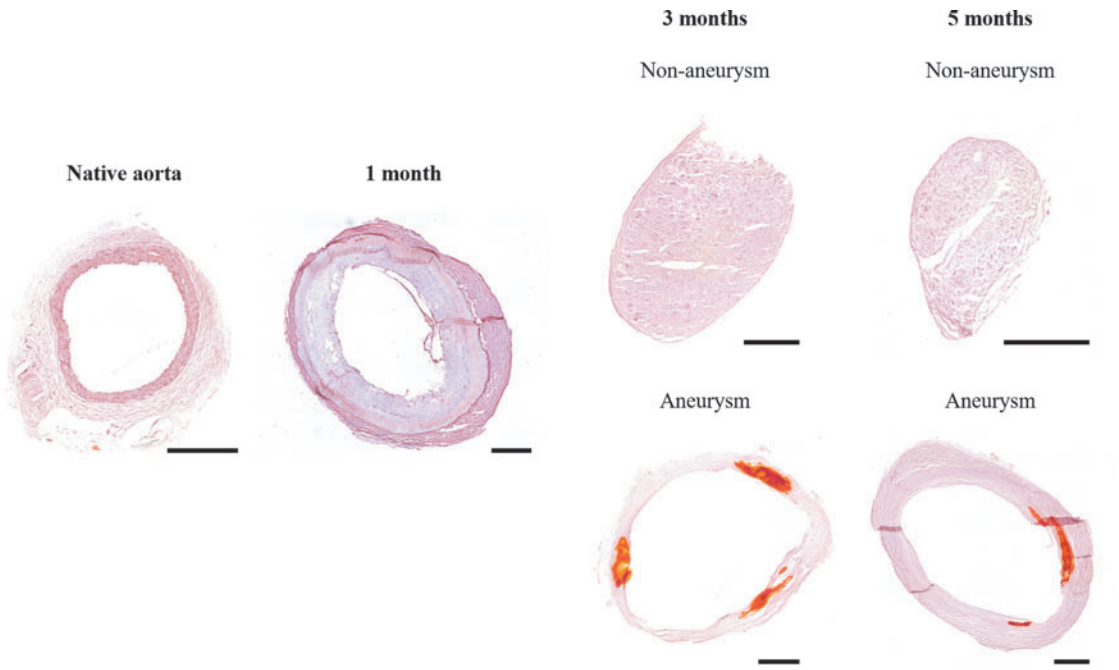

FIG. 5. Calcium presence. Alizarin Red S staining. Scale bars represent 500 μm.

a more tissue-like nonlinear elastic behavior in time, consistent with native vessels (Fig. 6).

Analysis of the nonaneurysmatic explants suggests that absence of endothelium leads to smooth muscle cell proliferation

α-SMA was present in all 3 and 5 months explants and to a lesser extent in 1 month explants (Fig. 7). A positive expression of vWF was found on the luminal surface of almost all explants, except for the explants that did not exhibit dilatation. This absence of endothelium was accompanied by increased smooth muscle cells (SMCs) (Fig. 7).

After 3 months in vivo *no polymer is detected in explants*

To determine the molecular weight of the remaining scaffold, explants were analyzed by GPC. As a control, sterile nonimplanted scaffolds were used. GPC analyses revealed that the remaining polymer scaffold in 1 month explants displayed a modest decrease in molecular weight as compared with the control (53.0 ± 1.0 kg/mol vs. 54.2 ± 0.2 kg/mol). The polymer dispersity index remained constant (2.05 vs. 2.06). GPC analyses of 3 and 5 months explants could not be conducted, as no scaffold material was present at these time points.

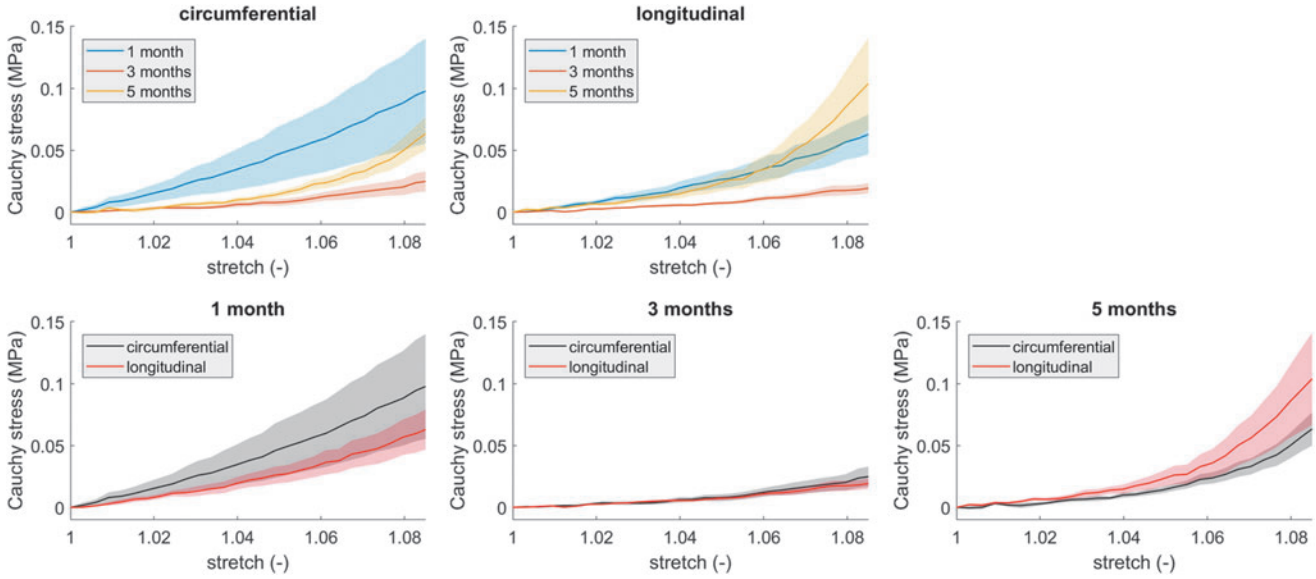

FIG. 6. Mechanical behavior of explants in time, as determined from biaxial tensile tests on the 1-, 3-, and 5-month explants. Data represent mean (*solid lines*) ± standard error of the mean (*shaded areas*).

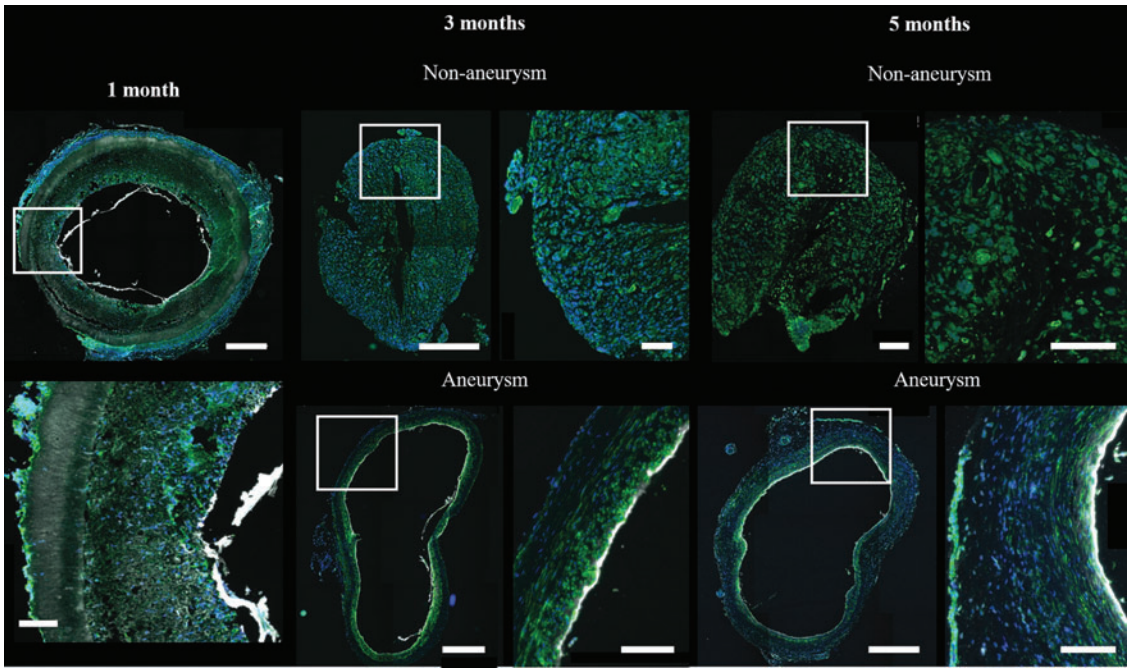

FIG. 7. Endothelium and smooth muscle cells. Cell nuclei in *blue*, von Willebrand Factor (endothelium) in *white*, and alpha smooth muscle actin (smooth muscle cells) in *green*. Scale bars represent 500 μm for the cross-sections of explants (images with a box). Scale bars represent 100 μm for the zoom images of explants (images without a box).

Discussion

The failure or success of material-based *in situ* vascular TE heavily relies on the ability to maintain mechanical integrity during the transition from scaffold to fully autologous neotissue in which no synthetic material is present. The host intrinsic regenerative capacity plays a major role during this process, as it is the key driving force behind neotissue formation and scaffold degradation. Next to material choice and scaffold design, a thorough understanding of material-driven vascular regeneration in an *in vivo* hemodynamic environment is therefore of pivotal importance in the ongoing quest to achieve mechanically stable vascular constructs. As the complex mechanical performance of the targeted vascular tissue sprouts from its multilayered and multifunctional microstructure, there is growing attention for designing multilayered scaffolds.[21–25] Following this multilayered approach, we designed a bioresorbable, bilayered scaffold—consisting of a porous inner layer for cell infiltration and a dense outer layer to provide strength—and investigated the *in vivo* performance of this scaffold to obtain understanding and handles for design optimization with respect to tissue development and tissue mechanical stability.

The main observation of this study is the variability in graft outcome despite homogeneity in the experimental group and scaffold production. Overall, we observed that in terms of mechanical properties, grafts with initial almost linear elastic behavior evolved toward nonlinear elastic behavior consistent with native vasculature.[26] Although many grafts failed (e.g., aneurysmal deformation, presence of calcium), a few showed no aneurysmal formation, a well-developed wall, and better mechanical performance. When analyzing these grafts in comparison with their failing counterparts, some striking differences were observed. First, these grafts had thicker and seemingly more contractile walls, which apparently developed in the absence of an endothelial covering. Second, two of three appeared to have been implanted in a prestretched configuration, as their length had increased in time, while failing grafts remained at their original length. Third, no calcium was present in nonaneurysmatic grafts, suggesting absence of adverse remodeling. Although these parameters cannot predict how the vascular wall will evolve with time and whether it will remain functional, they provide relevant handles to better understand variability in engineered tissue outcomes.

Our study is not the first that describes inconsistencies in graft outcome within a homogeneous experimental group. Khosravi *et al.* reported differences in graft stiffness of identical PGA-P(CL/LA)-based scaffolds that were implanted into the inferior vena cava in mice.[27] They suggested a different ratio in collagen types I and III attributed to the difference in stiffness. This could be due to different mechanical cues received by the cells, which consequently led to different extracellular matrix (ECM) deposition and remodeling. A possible explanation could be the prestretched configuration in which a graft is sutured into the native vasculature, which might contribute to different long-term outcomes. Although in this study all surgeries were performed by the same surgeon, small differences in this so-called prestretch might have contributed to inconsistencies in graft outcome, calling for the use of standardized surgical procedures and deeper insights into the effects of these on graft outcomes.

Hemodynamic forces are important regulators in vascular remodeling and homeostasis. Cells respond to changes in

their biomechanical environment by ECM remodeling to promote mechanical homeostasis.[28–30] Vascular smooth muscle cells (VSMCs) located in the media respond to alterations in hemodynamics by changing their phenotype. To induce vascular growth and remodeling, VSMCs differentiate into a synthetic phenotype. When tissue homeostasis is achieved, they switch back to a contractile phenotype to regulate vascular tone and overall vascular functionality.[31,32] A study by Loerakker *et al.* investigated the impact of mechanics on vascular homeostasis by combining cell experiments and computational modeling.[33] Their model predicted that the onset of VSMC differentiation from synthetic toward contractile VSMCs depended on the thickness of the VSMC layer, which might represent a homeostatic mechanical state.[33] In this study, we observed that nonaneurysmatic explants exhibited thicker walls and appeared to be more muscular, which might suggest that they are trying to achieve a vascular mechanical homeostatic state. Although the precise biological mechanisms that govern mechanical homeostasis remain unknown, we anticipate that these play a much bigger role than expected, resulting in either healthy or pathological vascular remodeling.

The endothelium plays a dynamic and strategic role in modulating vascular homeostasis, for example, through regulation of SMC proliferation. Endothelial cells have been shown to inhibit VSMC proliferation and support the contractile VSMC phenotype.[31,34] In this study, we observed that explants lacking an endothelium demonstrated a thicker VSMC layer compared with explants with endothelium. In the absence of endothelium, VSMCs are directly exposed to blood-flow-induced vascular wall shear stresses. Wall shear stress is known to regulate VSMC function by inducing a change in phenotype.[35] *In vitro* studies have demonstrated that VSMC proliferation is inhibited by high shear stress and promoted by low shear stress.[35,36]

In addition to its role in modulating vascular homeostasis, an endothelial layer is considered a prerequisite for successful *in situ* vascular TE, as it provides a nonthrombogenic surface.[37] Even though some explants lacked an endothelial layer, all remained patent throughout the duration of the study.

In addition to the well-accepted roles of wall shear stress and circumferential stress, axial wall stress has been advocated/suggested to play a contributing role in arterial biomechanics and mechanobiology.[38] In response to changes in blood flow or pressure, arteries can compensate for these changes through a reduction in axial stretch by increasing arterial length.[38] This supports the concept of the artery's capacity to adapt to hemodynamic changes to return toward mechanical homeostasis. In this study, we observed lengthening of nonaneurysmatic explants, which might suggest compensatory adjustment in an attempt to achieve mechanical homeostasis.

One of the challenges in arterial TE is to avoid aneurysmal dilatation, which often leads to fatal rupture.[39] This common complication is likely the result of insufficient structural stiffness of the neoartery during scaffold degradation. Slow degrading scaffolds provide mechanical support and prevent graft rupture, but could lead to adverse remodeling phenomena, such as calcification due to a prolonged presence of the scaffold.[40] To avoid these phenomena, fast degradation of scaffolds has been suggested for successful blood vessel regeneration *in situ*.[22] To date, studies that reported successful artery regeneration *in situ*, however, have used scaffolds that were reinforced with slow or nondegradable materials.[22,41] This could have ensured the reported short-term functional performance, but may result in long-term adverse effects such as calcification. In this study, we therefore designed a bilayered scaffold made of fast-intermediate degrading PC(e)-BU material where the dense outer layer was used to strengthen the scaffold. *In vitro* biaxial tensile testing confirmed that the dense outer layer greatly attributed to the strength of the graft. In time, we observed that all explants became stiffer *in vivo* in both longitudinal and circumferential directions. We did not observe differences in mechanical properties of the wall of nonaneurysmatic and aneurysmatic grafts, suggesting that this was not the direct cause of aneurysmal dilatation. However, the PC(e)-BU material, including the material located in the dense outer layer of the grafts, degrades within a time period of 1–3 months (see GCP data). Aneurysms are mostly visible as of the 3-month time point, so presumably these are caused by breakdown of the graft due to degraded or even absent synthetic material.[11] Aneurysms appear randomly stochastically at points where the grafts are initially weakest, and this can be anywhere across the graft (although Fig. 2A may suggest that the aneurysms are mostly located at the top half of the grafts). Within the time frame of this study, insufficient neotissue within grafts was formed. As the degradability of the implanted synthetic material can be tuned, for example from the fast-intermediate degrading PC(e)-BU that is used in this study to the slow degrading PC-BU material, either for the porous inner layer and/or for the dense outer layer, this offers several design handles to optimize scaffold architecture for future examinations to allow more robust neotissue formation.[11,42]

Safe clinical translation of TEVGs in the arterial circulation is still hampered by unpredictable graft outcomes. Studying variability in outcomes (e.g., implantation, host response, scaffold degradation, *etc.*) might provide the necessary cues for scaffold optimization, rather than incrementally optimizing scaffolds from just a mechanically or biological point of view. Improved mechanistic understanding of the biological mechanisms that govern scaffold-driven arterial regeneration and mechanical homeostasis is warranted to optimize materials and scaffolds. Future studies combining *in vivo* outcomes and numerical simulations could provide further insight into the relationship between scaffold implantation length, intrinsic tissue tension, and tissue outcome, thus providing handles for improved graft outcomes.[43–45] Analysis of the differences between preclinical successes and failures, as is done in this study, provides initial handles for scaffold optimization to improve future graft performance *in vivo*.

Acknowledgment

The authors thank Rik Tinnemans from Maastricht University for his assistance during the *in vivo* experiments.

Disclosure Statement

No competing financial interests exist.

Funding Information

This work was supported by a grant from the Dutch Government to the Netherlands Institute for Regenerative Medicine (NIRM, Grant No. FES0908).

References

1. Mathers, C., Stevens, G.A., Mahanani, W.R., Fat, D.M., and Hogan, D. Global Health Estimates 2016: Deaths by Cause, Age, Sex, by Country and by Region, 2000–2016. Geneva: World Health Organization, 2018.
2. Chlupác, J., Filová, E., and Bačáková, L. Blood vessel replacement: 50 years of development and tissue engineering paradigms in vascular surgery. Physiol Res **58,** S119, 2009.
3. Sabik, J.F., Lytle, B.W., Blackstone, E.H., Houghtaling, P.L., and Cosgrove, D.M. Comparison of saphenous vein and internal thoracic artery graft patency by coronary system. Ann Thorac Surg **79,** 544, 2005.
4. Klinkert, P., Post, P.N., Breslau, P.J., and van Bockel, J.H. Saphenous vein versus PTFE for above-knee femoropopliteal bypass. A review of the literature. Eur J Vasc Endovasc Surg **27,** 357, 2004.
5. Pashneh-Tala, S., MacNeil, S., and Claeyssens, F. The tissue-engineered vascular graft—past, present, and future. Tissue Eng Part B Rev **22,** 68, 2016.
6. Isenberg, B.C., Williams, C., and Tranquillo, R.T. Small-diameter artificial arteries engineered in vitro. Circ Res **98,** 25, 2006.
7. Collins, P., Webb, C.M., Chong, C.F., and Moat, N.E. Radial artery versus saphenous vein patency randomized trial: five-year angiographic follow-up. Circulation **117,** 2859, 2008.
8. Haruguchi, H., and Teraoka, S. Intimal hyperplasia and hemodynamic factors in arterial bypass and arteriovenous grafts: a review. J Artif Organs **6,** 227, 2003.
9. Li, S., Sengupta, D., and Chien, S. Vascular tissue engineering: from in vitro to in situ. Wiley Interdiscip Rev Syst Biol Med **6,** 61, 2014.
10. Wissing, T.B., Bonito, V., Bouten, C.V.C., and Smits, A.I.P.M. Biomaterial-driven in situ cardiovascular tissue engineering—a multi-disciplinary perspective. NPJ Regen Med **2,** 18, 2017.
11. van Haaften, E.E., Duijvelshoff, R., Ippel, B.D., *et al*. The degradation and performance of electrospun supramolecular vascular scaffolds examined upon in vitro enzymatic exposure. Acta Biomater **92,** 48, 2019.
12. Webber, M.J., Appel, E.A., Meijer, E.W., and Langer, R. Supramolecular biomaterials. Nat Mater **15,** 13, 2015.
13. Brunsveld, L., Folmer, B.J.B., Meijer, E.W., and Sijbesma, R.P. Supramolecular polymers. Chem Rev **101,** 4071, 2001.
14. van Almen, G.C., Talacua, H., Ippel, B.D., *et al*. Development of non-cell adhesive vascular grafts using supramolecular building blocks. Macromol Biosci **16,** 350, 2016.
15. Dankers, P.Y.W., Harmsen, M.C., Brouwer, L.A., van Luyn, M.J.A., and Meijer, E.W. A modular and supramolecular approach to bioactive scaffolds for tissue engineering. Nat Mater **4,** 568, 2005.
16. Bonito, V., Smits, A.I.P.M., Goor, O.J.G.M., *et al*. Modulation of macrophage phenotype and protein secretion via heparin-IL-4 functionalized supramolecular elastomers. Acta Biomater **71,** 247, 2018.
17. Ippel, B.D., Keizer, H.M., and Dankers, P.Y.W. Supramolecular antifouling additives for robust and efficient functionalization of elastomeric materials: molecular design matters. Adv Funct Mater **1805375,** 1, 2018.
18. Duijvelshoff, R., van Engeland, N.C.A., Gabriels, K.M.R., *et al*. Host response and neo-tissue development during resorption of a fast-degrading supramolecular electrospun arterial scaffold. Bioengineering (Basel) **5,** E61, 2018.
19. van Haaften, E.E., Bouten, C.V.C., and Kurniawan, N.A. Vascular mechanobiology: towards control of in situ regeneration. Cells **6,** E19, 2017.
20. L'Heureux, N., Dusserre, N., Konig, G., *et al.* Human tissue-engineered blood vessels for adult arterial revascularization. Nat Med **12,** 361, 2006.
21. Soletti, L., Hong, Y., Guan, J., *et al*. A bilayered elastomeric scaffold for tissue engineering of small diameter vascular grafts. Acta Biomater **6,** 110, 2010.
22. Wu, W., Allen, R.A., and Wang, Y. Fast-degrading elastomer enables rapid remodeling of a cell-free synthetic graft into a neo-artery. Nat Med **18,** 1148, 2012.
23. Hassan, K., Kim, S.H., Park, I., Lee, S.H., Kim, S.H., and Jung, Y. Small diameter double layer tubular scaffolds using highly elastic PLCL copolymer for vascular tissue engineering. Macromol Res **19,** 122, 2011.
24. Pham, Q.P., Sharma, U., and Mikos, A.G. Electrospun poly(epsilon-caprolactone) microfiber and multilayer nanofiber/microfiber scaffolds: characterization of scaffolds and measurement of cellular infiltration. Biomacromolecules **7,** 2796, 2006.
25. De Valence, S., Tille, J.-C., Giliberto, J.-P., *et al*. Advantages of bilayered vascular grafts for surgical applicability and tissue regeneration. Acta Biomater **8,** 3914, 2012.
26. Wagenseil, J.E., and Mecham, R.P. Vascular extracellular matrix and arterial mechanics. Physiol Rev **89,** 957, 2009.
27. Khosravi, R., Miller, K.S., Best, C.A., *et al*. Biomechanical diversity despite mechanobiological stability in tissue engineered vascular grafts two years post-implantation. Tissue Eng Part A **21,** 1529, 2015.
28. Cyron, C.J., and Humphrey, J.D. Vascular homeostasis and the concept of mechanobiological stability. Int J Eng Sci **85,** 203, 2014.
29. Humphrey, J.D., Dufresne, E.R., and Schwartz, M.A. Mechanotransduction and extracellular matrix homeostasis. Nat Rev Mol Cell Biol **15,** 802, 2014.
30. Humphrey, J.D. Vascular adaptation and mechanical homeostasis at tissue, cellular, and sub-cellular levels. Cell Biochem Biophys **50,** 53, 2008.
31. Renssen, S.S., Doevendans, P.A., and van Eys, G.J. Regulation and characteristics of vascular smooth muscle cell phenotypic diversity. Neth Heart J **15,** 100, 2007.
32. Halayko, A.J., and Solway, J. Molecular mechanisms of phenotypic plasticity in smooth muscle cells. J Appl Physiol **90,** 358, 2001.
33. Loerakker, S., Stassen, O.M.J.A., ter Huurne, F.M., Boareto, M., Bouten, C.V.C., and Sahlgren, C.M. Mechanosensitivity of Jagged-Notch signalling can induce a switch-type behavior in vascular homeostasis. Proc Natl Acad Sci USA **115,** E3682, 2018.
34. Beamish, J.A., He, P., Kottke-Marchant, K., and Marchant, R.E. Molecular regulation of contractile smooth muscle cell phenotype: implications for vascular tissue engineering. Tissue Eng Part B Rev **16,** 467, 2010.
35. Qiu, J., Zheng, Y., Hu, J., *et al*. Biomechanical regulation of vascular smooth muscle cell functions: from in vitro to in vivo understanding. J R Soc Interface **11,** 20130582, 2013.
36. Sterpetti, A.V., Cucina, A., D'Angelo, L.S., Cardillo, B., and Cavallaro, A. Shear stress modulates the proliferation

rate, protein synthesis, and mitogenic activity of arterial smooth muscle cells. Surgery **113,** 691, 1993.
37. Melchiorri, A.J., Hibino, N., and Fisher, J.P. Strategies and techniques to enhance the in situ endothelialisation of small-diameter biodegradable polymeric vascular grafts. Tissue Eng Part B Rev **19,** 292, 2013.
38. Humphrey, J.D., Eberth, J.F., Dye, W.W., and Gleason, R.L. Fundamental role of axial stress in compensatory adaptations by arteries. J Biomech **42,** 1, 2009.
39. Tara, S., Kurobe, H., Maxfield, M.W., *et al*. Evaluation of remodeling process in small-diameter cell-free tissue-engineered arterial graft. J Vasc Surg **62,** 734, 2015.
40. de Valence, S., Tille, J-C., Mugnai, D., *et al*. Long term performance of polycaprolactone vascular grafts in a rat abdominal aorta replacement model. Biomaterials **33,** 38, 2012.
41. Sugiura, T., Tara, S., Nakayama, H., *et al*. Novel bioresorbable vascular graft with sponge-type scaffold as a small-diameter arterial graft. Ann Thorac Surg **102,** 720, 2016.
42. Kluin, J., Talacua, H., Smits, A.I.P.M., *et al*. In situ heart valve tissue engineering using a bioresorbable elastomeric implant—from material design to 12 months follow-up in sheep. Biomaterials **125,** 101, 2017.
43. Szafron, J.M., Breuer, C.K., Wang, Y., and Humphrey, J.D. Stress analysis-driven design of bilayered scaffolds for tissue-engineered vascular grafts. J Biomech Eng **139,** 1210081, 2017.
44. Szafron, J.M., Khosravi, R., Reinhardt, J., *et al*. Immuno-driven and mechano-mediated neotissue formation in tissue engineered vascular grafts. Ann Biomed Eng **46,** 1938, 2018.
45. Szafron, J.M., Ramachandra, A.B., Breuer, C.K., Marsden, A.L., and Humphrey, J.D. Optimization of tissue-engineered vascular graft design using computational modeling. Tissue Eng Part C Methods **25,** 561, 2019.

Address correspondence to:
Carlijn V.C. Bouten, PhD
Department of Biomedical Engineering
Eindhoven University of Technology
P.O. Box 513
Eindhoven 5600 MB
The Netherlands

E-mail: c.v.c.bouten@tue.nl

Received: July 2, 2020
Accepted: August 28, 2020
Online Publication Date: October 5, 2020